Energy disposal by F atom abstraction reactions: HF vibrational–rotational distributions from F+HBr and HI

K. Tamagake, D. W. Setser, and J. P. Sung

Citation: The Journal of Chemical Physics **73**, 2203 (1980); doi: 10.1063/1.440416
View online: http://dx.doi.org/10.1063/1.440416
View Table of Contents: http://scitation.aip.org/content/aip/journal/jcp/73/5?ver=pdfcov
Published by the AIP Publishing

Energy disposal by F atom abstraction reactions: HF vibrational–rotational distributions from F+HBr and HI

K. Tamagake,[a] D. W. Setser, and J. P. Sung[b]

Department of Chemistry, Kansas State University, Manhattan, Kansas 66506
(Received 13 March 1980; accepted 15 May 1980)

HF infrared chemiluminescence from the reactions of F atoms with HCl, HBr, and HI was used to assign vibrational–rotational populations of the HF product. Experiments were done in both a cold-wall, arrested vibrational–rotational relaxation apparatus and in a fast-flow, arrested vibrational relaxation apparatus. Since the total HF formation rate constants are known for these reactions, absolute 300 K rate constants for formation of HF_{vJ} are established. The mean vibrational energy disposal to HF including estimates for HF ($v=0$) is $\langle f_V \rangle_{HCl} = 0.51$, $\langle f_V \rangle_{HBr} = 0.59$ and $\langle f_V \rangle_{HI} = 0.59$. The mean HF rotational energy decreased from 0.18 to 0.12 in the HCl–HI series. The $\langle f_V + f_R \rangle$ sum is virtually constant for the three reactions, but $\langle f_V \rangle$ does increase slightly as the reactions become more exoergic. The HBr reaction yields ~10% $Br(^2P_{1/2})$, the upper spin–orbit state; but $I(^2P_{1/2})$ is not formed from HI. Independent work by Nip and Clyne on the HCl reaction suggest that $Cl(^2P_{1/2})$ also is formed in ~10% yield. The dynamics of these reactions are considered with the aid of information-theoretic analysis. The possibility of two components, direct and complex, for product formation is considered. The HF vibrational distribution from the HBr and HI experiments in the cold-wall apparatus showed an unusual dependence upon reagent flow and the "best" distributions were not found for the lowest flow. The selection of the "best" initial vibrational populations were assisted by the data from the fast-flow apparatus, which included experiments with DCl and DBr as well as HCl, HBr, and HI.

I. INTRODUCTION

In previous work[1–3] from this laboratory the vibrational energy disposal for the hydrogen abstraction reactions by fluorine atoms from a series of polyatomic hydride molecules has been characterized. In some instances the steady-state rotational distributions[3] from the reagents suggested that interesting differences might exist in the rotational energy disposal. In studying the vibrational energy disposal, it was advantageous to compare results from reactions which ranged from the simple three-body case to those with hydrides of moderate complexity. As the first step in a systematic investigation of the rotational energy disposal for polyatomic reaction systems, it was decided to obtain data for some representative three-body reactions. The simplest possibilities are the hydrogen halide series, which subsequently will be used as reference reactions for comparison to rotational energy disposal of polyatomic cases:

$$F + HCl \rightarrow HF^{\dagger} + Cl(^2P_{3/2}), \quad \Delta H^{\circ}_0 = -32.8 \text{ kcal mol}^{-1}, \quad (1a)$$

$$\rightarrow HF^{\dagger} + Cl(^2P_{1/2}), \quad \Delta H^{\circ}_0 = -30.3 \text{ kcal mol}^{-1}, \quad (1b)$$

$$F + HBr \rightarrow HF^{\dagger} + Br(^2P_{3/2}), \quad \Delta H^{\circ}_0 = -48.5 \text{ kcal mol}^{-1}, \quad (2a)$$

$$\rightarrow HF^{\dagger} + Br(^2P_{1/2}), \quad \Delta H^{\circ}_0 = -38.0 \text{ kcal mol}^{-1}, \quad (2b)$$

$$F + HI \rightarrow HF^{\dagger} + I(^2P_{3/2}), \quad \Delta H^{\circ}_0 = -64.7 \text{ kcal mol}^{-1}, \quad (3a)$$

$$\rightarrow HF^{\dagger} + I(^2P_{1/2}), \quad \Delta H^{\circ}_0 = -43.0 \text{ kcal mol}^{-1}, \quad (3b)$$

where † denotes general vibrational–rotational excitation. This paper summarizes our efforts to obtain initial vibrational–rotational distributions for these reactions. A new cold-wall, low pressure, arrested vibrational–rotational relaxation vessel was constructed and a fast-flow, arrested vibrational technique was developed.[4] All infrared emission measurements in this work were made with a Digilab Fourier transform spectrometer which enhanced the sensitivity for detection of infrared emission by more than an order of magnitude relative to our earlier studies[1–3] utilizing a grating spectrometer. Preliminary results from studies of Reactions (1)–(3) with the fast-flow technique already have been reported.[4] We found that F + HBr gave 10% $Br(^2P_{1/2})$; but the formation of $I(^2P_{1/2})$ from Reaction (3b) was insignificant. Clyne and Nip[5] have independently measured 10% formation of $Cl(^2P_{1/2})$ from Reactions (1).

Reactions (1) were included as a test case for our technique since good data already are in the literature[6] for initial vibrational–rotational distributions. We were able to duplicate those results with relative ease. To our surprise it was much more difficult to obtain arrested rotational *or* vibrational distributions for Reactions (2) or (3). The best aspects of both the cold-wall and the fast-flow techniques were required to solve the problem. In particular, reducing the reagent flow rates in the cold-wall vessel below a certain level gave distributions which we interpret as being somewhat relaxed, probably as a consequence of scattering of HF_{vJ} from the walls of the cold-wall reaction vessel. This seriously complicates the interpretation of the results from the cold-wall experiments since at sufficiently high flow rates relaxation, of course, occurs from gas phase collisions. Data from the fast-flow apparatus for very low reagent concentrations in 0.7 Torr of Ar carrier gas were used to identify the correct initial $HF^{\dagger}$ vibrational distributions, which corresponded to data obtained from intermediate flow rates in the cold-wall experiments. Recently, Polanyi and co-workers[7] have reported on Reactions (2); they also found the peculiar variation of the relative HF_{vJ} populations with flow rate. However, they select the low flow rate results to derive initial HF_{vJ} distributions. In contrast Jonathan and co-workers[8] found little or no dependence of the steady-state $HF^{\dagger}$

[a] Present address: Faculty of Pharmaceutical Sciences, Okayama University, Okayama, Japan 700.

[b] Present address: Monsanto Textiles Co., Pensacola, Fla. 32504.

 0021-9606/80/172203-15$01.00

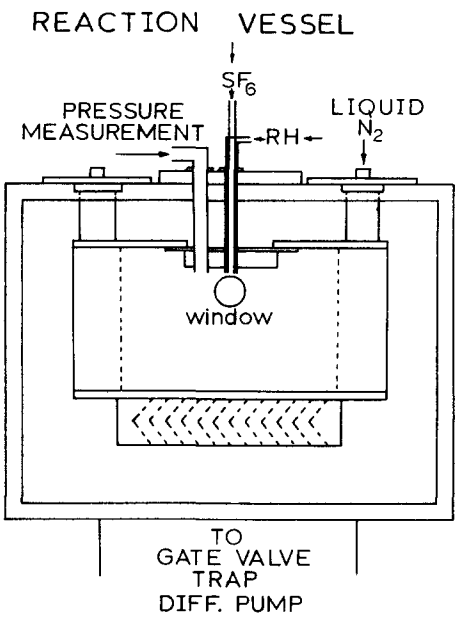

FIG. 1. Schematic drawing of the cold-wall arrested relaxation reaction vessel. The outer box was constructed from a 2.5 cm aluminum plate. The dimensions were $51\times72\times91$ cm. The inner box was constructed of high thermal conductivity aluminum and had dimensions of $22\times28\times42$ cm; the sides, top, and baffle were bolted to the liquid N_2 reservoirs. Aluminum tubing connected to the liquid N_2 reservoirs was welded to the aluminum plates that comprised the baffle. The inner box was sealed to the outer box via a double O-ring flange system using a stainless steel blank to minimize the heat transport between the two boxes at the points of suspension of the liquid N_2 reservoirs. We thank Dr. McDonald (University of Illinois) for advice on this aspect of the construction.

populations on reagent flow (in a cold-wall vessel) and report initial distributions in close agreement with those we favor as being the best distribution. In view of these interesting problems, we have presented a detailed report of our findings; the comparison of the results from the fast-flow reactor and those from the cold-wall vessel are of special importance.

As the final step in pinpointing the correct initial vibrational distribution and in ascertaining the branching ratio between Reactions (2a) and (2b), Reactions (4) were studied by the fast flow technique:

$$F + DBr \rightarrow DF^{\dagger} + Br(^2P_{3/2}), \quad \Delta H_0^\circ = -49.1 \text{ kcal mol}^{-1}, \quad (4a)$$

$$\rightarrow DF^{\dagger} + Br(^2P_{1/2}), \quad \Delta H_0^\circ = -38.6 \text{ kcal mol}^{-1}. \quad (4b)$$

The data from Reactions (4) support the branching ratio found earlier[4] for Reactions (2) and also support the assignment of $\langle f_V \rangle$ for the F + HBr reaction. In order to test the role of the thermochemical energy limit on formation of $HF(v=3)$ from Reactions (1), the F + DCl reaction also was investigated in the flow apparatus.

II. EXPERIMENTAL

Figure 1 shows our arrested relaxation cold-wall reaction vessel. The inner vessel was constructed from high thermal conductivity aluminum to ensure that all of the surface was at 95 K when the side compartments were filled with liquid N_2. Further details are given in the figure caption. A 10 in. diffusion pump and the cryopump maintained the pressure in the vessel at $(0.5-1.0)\times10^{-5}$ throughout the experiment. A concentric nozzle was used to mix the reagents and F atom produced by microwave discharge of SF_6. The diameters of the inner and the outer tubes of the concentric nozzle were 10 and 19 mm, respectively. The inner tube, which was alumina, extended 4 mm beyond the end of the outer tube. The microwave discharge usually was stable and it was not necessary to have a Teflon plug at the end of the inner tube. The flow rates of SF_6 and reagents were 2–10 and 5–100 μmol/s, respectively.

The Pyrex glass 5 cm i.d. flow vector used in the fast flow studies has been described elsewhere.[9–11] Briefly, F atoms, generated by microwave discharge in CF_4/Ar, were delivered to the central axis of the flow tube by an alumina tube. The alumina tube extended 12 cm into the flow tube. The reagents (highly diluted in Ar) were introduced by a 6 mm o.d. Pyrex tube which extended 15 cm into the flow tube and terminated in a glass ring near the edge of the observation window (a 55 mm NaCl window). The glass ring was constructed from a 3 mm Pyrex tube containing a number of small holes in the inside of the ring. A similar, but larger, glass ring at the beginning of the flow tube was used to introduce the majority of the carrier Ar. Water impurity in Ar was removed by passing Ar through four activated molecular sieve traps cooled to 196 K. The pressure in the flow tube was 0.75 Torr. The bulk flow velocity, provided by the Roots-type blower and a large mechanical pump, was 85 m/s. The concentrations used in the experiments were $[F] \cong 5\times10^{11}$ and $[HX] = 3.5-35\times10^{11}$ molecules cm^{-3}.

The HCl, HBr, and HI were taken from Matheson lecture bottles. Care must be taken to remove the $H_2/Br_2/I_2$ impurities from HBr and HI. Also, we found that some HBr and HI tanks contained rather high concentrations of HCl impurity. The DCl and DBr were prepared by standard synthetic methods.

The Digilab model FTS-20 interferometer was used with a liquid N_2 cooled InSb detector to record the spectra. The large throughput of the interferometer is advantageous for collecting weak emissions. However, the proper design of a multiple reflection cell is somewhat difficult because the light collection system tends to decrease the optical throughput unless very large mirrors or a very small reaction vessel are used. In our work a single reflecting mirror was used as the light collecting system.[12] This has several advantages. Throughput matching with the interferometer can be easily achieved, the mirror outside of the reaction vessel is easy to keep clean, and the alignment is easy to maintain.

Two InSb detectors were used. One had a built-in filter which sharply cut off frequencies lower than 3600 cm^{-1}. The other had no filter and the response extended to 1750 cm^{-1}. The filtered detector had a five times better S/N ratio at ~3700 cm^{-1} since the major portion of the thermal emission, which causes scintillation noise proportional to the square root of the photons striking

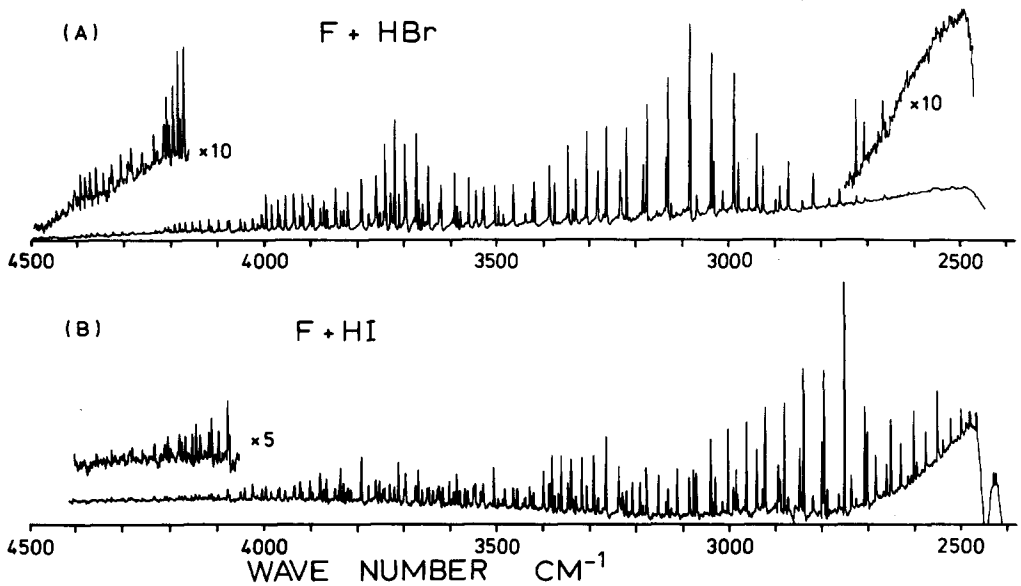

FIG. 2. $HF^{\dagger}$ emission spectrum from F+HBr and F+HI (experiments 7 and 12 of Table I, respectively).

the detector, was removed. The filtered detector was used for some studies to observe $HF(v \leq 3)$. However, for most HBr and HI experiments the broad-band detector was used in order to observe the emission from the P-branch lines of $HF(v=4-6)$. For the broadband detector the thermal emission from the environment was so intense at low frequency (below 2200 cm^{-1}) that the A–D converter was saturated at the central burst peak of the interferogram when the proper amplifier gain was used for the very weak HF emission. It was necessary to remove the thermal emission by adding a filter; we placed a 1 mm plate of glass (or quartz in later work) in front of the detector. This plate removed the thermal radiation below 2200 cm^{-1}. Although no improvement could be expected in the scintillation noise because the glass filter still is at room temperature and emits radiation at low frequency (which, however, is not a function of the position of the moving mirror unlike the radiation absorbed by the glass filter), the net improvement of the S/N ratio was a factor of 2.

The entrance aperture to the interferometer was placed at the focal point of the collimating mirror. The size of the aperture was varied, depending upon the desired resolution, so that the aperture limiting resolution $\Delta\nu \simeq h^2\nu/8F^2$ is much smaller than the retardation limiting resolution $\Delta\nu \simeq (1/L)^4$, where h, F, and L are the diameter of the aperture, the focal length of the collimating mirror, and the maximum optical displacement of the moving mirror, respectively. Under such condition, the resolution or the width of a single emission line would be constant throughout the wave number region below 5000 cm^{-1}. For most experiments, 2 cm^{-1} of resolution was used to resolve the lines of the HF vibrational-rotational spectra. Adding of three points by interpolation at the plotting stage assured the accuracy of the peak heights which were used to obtain relative populations. Two sample spectra are shown in Fig. 2.

The correction curve for the spectral response of the interferometer, other optics, and detector was obtained using a black body radiation cavity at 1000°C. In order to avoid saturation of the detector, the total intensity of the source must be attenuated. This was accomplished by placing an aluminum foil pierced with several pin holes between the detector and interferometer block. Einstein coefficients for HF were calculated based on a dipole moment function and the numerically computed vibrational wave function of HF. These Einstein coefficients are described and listed elsewhere.[12]

At the early stage of this work, difficulties were encountered in obtaining good line shapes in the Fourier transformed spectrum. When the flow rate of reagent was high and the emission was much stronger than the background, the spectrum was acceptable, although some weaker lines were slightly skewed. However, as the intensity was decreased by reducing the reagent flow, the line shapes became skewed severely. Further reduction of the flow rate caused all emission lines to appear in the negative direction. This was so severe that the spectrum had the appearance of an absorption spectrum. Other laboratories have found similar line shape problems when examining weak emission lines with an interferometer. The explanation favored in our laboratory, but not in all others, is that thermal emission from the detector housing is reflected by the interferometer and returned to the detector element, this affects the selection of the phase in the computational routine, and for very weak signals the phase is in error by up to 180°. Manual phase correction or subtraction of the background interferogram before doing the Fourier transform was effective in obtaining improved spectra. A discussion of this problem has already been reported[13(a)] and a detailed analysis will appear elsewhere.[13(b)]

III. RESULTS

A. Experimental conditions for arrested relaxation

The $HF^{\dagger}$ vibrational–rotational populations from the F + HCl reaction were examined in order to judge the

TABLE I. Vibrational populations in the cold-wall reactor for various flow rates.

Experiments	Reagent	f_{RH} (μmol s^{-1})	f_{SF_6} (μmol s^{-1})	Vibrational distribution P_v					
				v_1	v_2	v_3	v_4	v_5	v_6
1	HCl	20	4.7	0.41	0.54	0.06			
2		68	11	0.29	0.60	0.10			
3		135	11	0.25	0.64	0.11			
4[a]	HBr	6.8	2.7	0.48	0.27	0.15	0.10		
5		6.8	2.7	0.36	0.23	0.20	0.21		
6		6.8	11	0.13	0.15	0.30	0.42		
7		14	15	0.12	0.17	0.30	0.41		
8[b]		34	11	0.06	0.23	0.31	0.41		
9		34	15	0.17	0.19	0.28	0.36		
10		170	11	0.14	0.18	0.30	0.38		
11	HI	3.4	2.7	0.22	0.19	0.17	0.14	0.15	0.13
12		6.8	11	0.10	0.11	0.13	0.16	0.22	0.28
13		14	14	0.12	0.12	0.13	0.16	0.21	0.27
14		100	11	0.12	0.14	0.15	0.18	0.21	0.21
15	H_2S	1.4	2.7	0.36	0.29	0.24	0.12		
16		11	0.8	0.33	0.27	0.27	0.13		
17		6.8	2.7	0.27	0.27	0.30	0.16		
18		2.7	20	0.23	0.25	0.34	0.18		
19	CH_3Cl	6.8	15	0.17	0.41	0.42			
20		34	11	0.10	0.34	0.56			
21		68	11	0.09	0.36	0.55			
22		20	11	0.11	0.34	0.55			

[a]All experiments except for #4 (separated nozzles) were done with the concentric nozzle arrangement shown in Fig. 1.

[b]This spectrum was very noisy and it was difficult to measure high J lines of $v=1$; the relative populations are less reliable than others.

effectiveness of our arrested relaxation vessel and to ascertain the optimum experimental conditions. The vibrational–rotational populations[1] were in good agreement with the published values,[5] when the flow rates were 65–160 μmol s^{-1} for HCl and 3–12 μmol s^{-1} for SF_6. These flow rates are higher than the values used in other works.[6–8] However, the relatively large size of the nozzles and the larger surface area of the inner box of our apparatus keeps the pressure in the reaction zone low in spite of the high flow rates. When we used HCl flow rates lower than ~20 μmol s^{-1}, in an attempt to obtain less relaxed rotational populations, the $v=1$ population increased unexpectedly (see Table I). This phenomenon was observed even more clearly when HCl was replaced by HBr or H_2S, because these molecules have much higher rate constants and the flow rate could be reduced to 1.5 μmol s^{-1} and still observe emission. In each case reducing the flow rates below a certain limit caused the $v=1$ and 2 populations to increase sharply, whereas the rotational populations for high vibrational levels ($v=3$ and 4) tended to be slightly more arrested at the lowest flow rates. Polanyi's group[7] observed [See note added in proof] the same trend in HF† populations with variation of the HBr flow rate in the Monel vessel, so the effect is not unique to our aluminum vessel. Polanyi and co-workers suggested that secondary processes affected the distributions at intermediate and high flow rates and concluded that the experiments with lowest flow rate gave the best estimate of the initial populations. In our opinion, secondary reactions or energy pooling even at the highest flow rate are negligible in our experiments; the lack of HF emission from levels exceeding the thermochemically allowed energy provides some support for this claim.

In order to resolve the discrepancy found in the arrested relaxation vessel, independent experiments were done in the fast-flow reactor with the lowest flows of F atoms (microwave discharge of CF_4/Ar or SF_6/Ar mixtures) and reagent that could be used and still obtain satisfactory emission intensities. These results are described in Sec. III B. For every case in question shown in Table I, the vibrational distributions from the fast-flow reactor support the distributions obtained from the mid-flow rate range of experiments in the cold-wall apparatus.

Possible explanations for the increase of the low v level populations for very low flow rates could be either or both of the following effects: One is a wall effect. Trapping by the surface of a wall that is coated with SF_6 may not be so effective that each wall collision traps an HF† molecule with 100% efficiency at 77 K. The HF molecules that rebound from the surface may be partially or completely vibrationally relaxed. If these HF molecules re-enter the observation zone, they can emit radiation or collide with other HF† molecules causing relaxation. In either case an abnormal increase of the $v=1$ and 2 population will occur. Perhaps the high reagent flow rates prevent the "old" molecules from entering the observation area which is being continually swept out by the flow of reagent from the nozzle. Although the high flow rates may cause significant rotational relaxa-

TABLE II. Vibrational distributions[a] from fast-flow reactions.

Reagent	Vibrational distribution[b] P_v						Fraction in $J \geq 10$
	v_1	v_2	v_3	v_4	v_5	v_6	
HCl	0.25	0.63	0.11				None observed
DCl[d]	0.11	0.34	0.45	0.10			None observed
HBr[c]	0.09	0.22	0.34	0.35			0.10
DBr[d]	0.06	0.13	0.17	0.22	0.24	0.18	None observed
HI[c]	0.10	0.15	0.18	0.22	0.23	0.12	0.14
CH_4	0.18	0.66	0.17				None observed
C_2H_6	0.11	0.49	0.40				None observed
CH_3Cl	0.07	0.33	0.59				None observed
CH_3Br	0.11	0.39	0.50				None observed
H_2CO[e]	0.13	0.25	0.38	0.23			0.14
H_2S	0.22	0.37	0.31	0.10			0.10
SiH_4	0.17	0.30	0.41	0.12			0.17
GeH_4	0.11	0.20	0.30	0.35	0.04		0.18

[a]These distributions were obtained for the lowest [F] and [RH] that could be used and still obtain reliable signals. These typically were $[F] \approx 5\times10^{11}$ and $[RH] = 2\times10^{11}$ molecules cm^{-3}.
[b]These are the total contribution to each v level including the high J component.
[c]The distributions reported in Ref. 4(b) were 0.10/0.23/0.33/0.34 for HBr and 0.11/0.16/0.18/0.21/0.20/0.14 for HI.
[d]The Einstein coefficients for DF were computed using the same method as employed previously[12] for HF.
[e]This distribution supersedes that reported in Refs. 1 and 3, the earlier results (cold-wall experiment) suffered from relaxation and/or secondary reactions.

tion, the vibrational populations usually will not be relaxed by the small number of gas phase collisions. A second explanation is that at very low pressures (low flows) the $HF^\dagger$ molecule formed at a long distance from the observation area may come into the field of view after collisional and/or radiative relaxation, i.e., the effective reaction zone could be larger than the geometric observation zone. The existence of some type of wall effect is supported by the fact that the flow effects were not observed for F atoms with noncondensible reagents such as H_2, CH_4, or C_2H_6 for which the minimum pressures at 77 K were 10^{-4} Torr. Also, no effects were found for H atom reactions with halogens or sulfur chlorides[11,12] for which a flow of H_2 maintains a minimum background pressure of $\sim10^{-4}$ Torr. The flow effect was only noticed for *fast* reactions which permitted very low flow rates of condensible (at liquid N_2 temperature) reagent and F atom source (SF_6). In spite of the admitted ambiguity of our explanation, we prefer the medium flow rate experiments, which gave the low $v=1$ populations, as providing the "best" initial vibrational distributions for the 300 K reaction. The best rotational distributions for the high v levels are taken from the low flow rate experiments. For the lower v levels highly arrested rotational distributions could not be obtained (except for F + HCl) and the best rotational distributions are from the same experiments giving the best vibrational distributions. Actually, the data[4(b)] from the fast-flow reactor also provide good evidence for the envelope of the initial HF ($v=1$ and 2) rotational distributions for Reactions (2) and (3).

B. HF distributions form the fast-flow reactor

Our initial study of HF infrared chemiluminescence from the fast-flow reactor utilized a grating monochromator.[14] In order to obtain adequate intensities the reagent and F atom concentrations were higher than desirable and in some cases a moderate degree of vibrational relaxation did occur, although this had little effect upon the primary concern, the measurement of relative rate constants. Subsequently, the use of the increased sensitivity of the interferometer permitted the reduction of F (from 5×10^{12} to 5×10^{11} molecules cm^{-3}) and reagent (from the 10^{12} to the 10^{11} molecules cm^{-3} range) concentrations. Except for reagents with superfast vibrational relaxation rates or for slow reactions which require high reagent concentration, initial vibrational distributions usually can be observed[4,9,10] at the first observation window (0.2 ms of reaction time). There is some evidence that relaxation *may* not be fully arrested for very high v levels, i.e., $HF(v \geq 6)$ under the conditions currently used. However, this point is not yet settled. If $HF^\dagger(v=1-3)$ is formed in high rotational levels ($J \geq 10$), even the residue of the initial high J populations can be observed.[4(b)] The kinetics in the fast-flow reactor are more thoroughly discussed in Ref. 10. Table II presents a summary of the vibrational distributions and the total fraction of the population with $J>10$ observed with the best technique developed for the fast-flow reactor. All the F atom reactions that have been reinvestigated, as well as HBr, HI, H_2S, and CH_3Cl, which are of specific interest for comparison to Table I, are included in Table II. Except for HBr and HI, the results of Table II are based on the same data discussed in Ref. 4(b). The new results for HBr and HI are in good agreement with the distributions listed in Ref. 4(b). The steady-state HF distributions given in Fig. 3 from F + HBr show the high J components; the $J>10$ fractions are 0.30, 0.18, 0.07, and 0.01 for $v=1$, 2, 3, and 4, respectively. For HI the fractions are 0.20, 0.30, 0.22, 0.13, 0.04, and 0.00 for $v=1$, 2, 3, 4, 5, and 6, respectively.

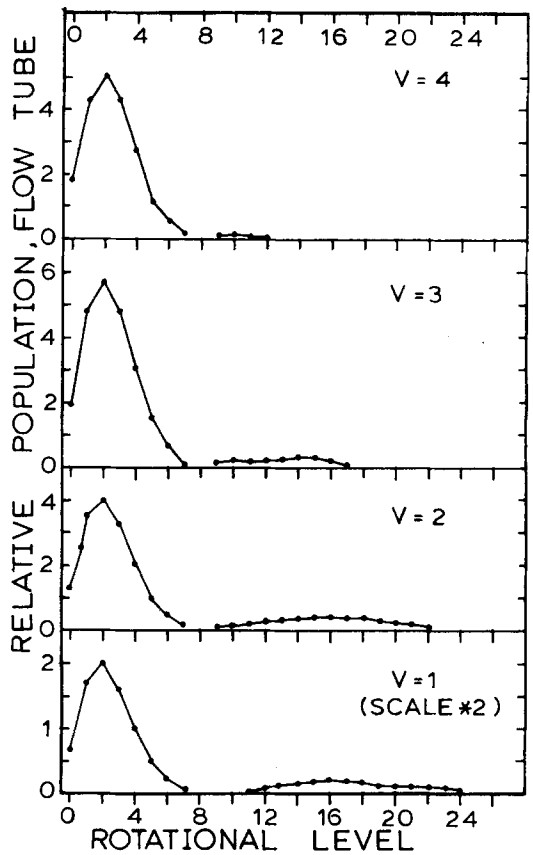

FIG. 3. The $HF^{\dagger}$ vibrational–rotational distributions from F + HBr in the fast-flow apparatus. The $J > 10$ populations are 30%, 18%, 7%, and 1% for $v = 1$, 2, 3, and 4, respectively. Note that the most probable J value in the envelope of the high rotational distributions coincides with the most probable J in the initial distributions of Fig. 4. The scale for $v = 1$ has been expanded by two for convenience of presentation.

Experiments in the flow reactor also were done with DBr and DCl. The DF vibrational distributions were independent of DBr or DCl flow and the average of several experiments is shown in Table II. Comparisons were made of the DF($\Delta v = 1$), HF($\Delta v = 1$), and the $Br(^2P_{1/2}$–$^2P_{3/2})$ emission intensities from Reactions (3) and (4). Within the considerable experimental error (±100%), the $Br(^2P_{1/2}$–$^2P_{3/2})$ emission intensity was the same for both HBr and DBr. In the new work no effort was made to remeasure the ratio of $Br(^2P_{1/2}$–$^2P_{3/2})$ to HF emission intensities quantitatively; however, on a qualitative basis the $Br(^2P_{1/2})$ emission intensity was consistent with the earlier report[4(a)] and we believe that our former measurements are correct in spite of work finding contrary results.[15] Polanyi's group[7] has reported that 7% ± 3% of the HF is formed by Reaction (2b), which compares well with our earlier estimate[4(a)] of 10% ± 4%.

Since our report[4(b)] of the relative rate constants for HCl, HBr, and HI, two other studies have been published.[5,16] We also discovered that the HBr and HI tanks previously used were contaminated (~10%) with HCl. Although this contamination has little effect on our rate constant measurements,[4(b)] we decided to remeasure the relative rate constants for the CH_4/H_2, CH_4/HCl, CH_4/HBr, and HBr/HI pairs, with inclusion of the high J components, which could not be observed in earlier studies using the monochromator. Since the individual vibrational–rotational lines are fully resolved and the variation of the Einstein coefficients are explicitly considered, the present measurements should be more reliable. In each case the results were obtained by comparing the slopes of the plots of $\sum HF_{vJ}$ relative concentrations vs reagent concentration. The new results are summarized in Table III, together with the results of Refs. 4(b) and 16(a). There is moderately good agreement among the studies; the HBr and HI reactions evidently have nearly equal rate constants, which are ~5 times larger than the value for the HCl reaction. Very recent measurements by Wurzberg and Houston[16(b)] emphasize the strongly non-Arrhenius temperature dependence of the F + HX rate constants.

In the present work the most important aspect of the fast-flow results is the identification of the initial P_v(HF) via comparison of Tables I and II. For HCl the fast-flow and the cold-wall, high flow experiments are in perfect agreement. For HBr the agreement between experiments 10, 9, 6, and 7 of Tables I and II are satisfactory, although $v = 4$ population in the cold-wall vessel appears to be significantly higher than in the flow reactor. The P_v(HF) from the lowest flow rate experiments 4 and 5 are obviously different and, as discussed in Sec. III A, we believe these are not relevant for assigning initial vibrational distributions. The P_v(DF) from F + DBr are in very good agreement with P_v(HF) (on a P_v vs f_V plot) from the fast-flow experiments, which provides general support for these being close the initial HF(v) distribution from F + HBr. Except for the highest level v_6, the F + HI distributions in Tables I (experiments 12 and 13) and II are in close agreement. Any relaxation in the fast-flow reactor would affect the highest level most severely and this may explain the small difference for HF($v = 6$). The three higher flow cold-wall experiments are in good agreement with the fast-flow results for $F + CH_3Cl$. The two higher flow H_2S experiments 17 and 18 of Table I are in modest agreement with the fast-flow P_v of Table II. These H_2S distributions also are in close agreement with a recent cold-wall arrested relaxation study by Dill and Heydtmann[17] ($v_1/v_2/v_3/v_4 = 0.26/0.33/0.27/0.14$).

C. Vibrational-rotational distributions from HBr

The fundamental region of the spectrum observed from experiment 7 of Table I is shown in Fig. 2. The populations deduced from the spectrum are shown in Fig. 4. The highest observed levels are $J = 13$ of $v = 4$ and $J = 19$ of $v = 3$ both are coincident with the mean available energy of the F + HBr reaction. The best conditions for determining the initial vibrational distribution are similar to those of experiment 7. Boltzmann-like rotational distributions are found for low J of each vibrational level, but the degree of rotational relaxation of each v level seems to be somewhat different. The low J components for $v = 3$ and 4 become even smaller when the reagent flow rates were reduced, which is normal if the low J populations increase due to rotational relaxation by collisions with reagent. However, as already discussed, the low J level population for $v = 1$ and 2 in-

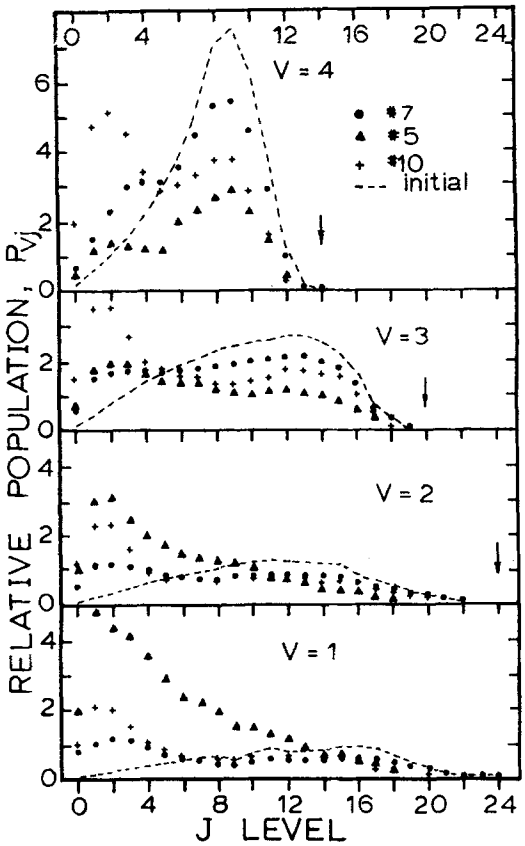

FIG. 4. The HF_{vJ} distributions from F+HBr for cold-wall experiments 5, 7, and 10. The dashed line shows our estimate of the initial distributions. Experiment 7 represents the intermediate flow, less relaxed cases; experiment 5 shows the apparent relaxation at lower flows; experiment 10 illustrates the apparent onset of relaxation at the highest flows. The $\sum_v \sum_J P_{vJ}$ is normalized to 100 for each experiment. The small vertical arrows identify the highest energetically allowed J level.

creased when the flow rates were reduced (as illustrated by experiment 5 in Fig. 4) just as the $v=1$ and 2 vibrational populations increased for low flow rates. The abnormal behavior of the low J populations of $v=1$ and 2 is another reason why we consider the low flow rate experiments as not giving true initial populations. Many experiments confirmed that the behavior of the rotational distributions is almost always described by the above statements for experiments done on the same day; but if experiments from different days are compared, it is difficult to say anything quantitative about the dependence of rotational distribution upon flow rates. Rotational distributions depended upon not only flow rates but also on the nozzle configuration and possibly other unknown factors such as the cleanliness of the wall surface.

For ease of separation of rotationally relaxed components from the initial rotational population, $\ln[P_{vJ}/(2J+1)]$ were plotted against $J(J+1)$, which is proportional to the rotational energy. The plot is expected to be linear at low J, if the relaxed components are Boltzmann-like, and to be more flat in the mid-J region corresponding to the initial distribution. Consequently removing relaxed components by extrapolation will be easier than on a $P_{v,J}$ vs J plot. As shown in Fig. 5, the slopes of

TABLE III. Relative 300 K rate constants for F+HX.

Molecule	This work[a]	Sung and Setser[b]	Wurzberg *et al.*[c]	Nip and Clyne[c]
CH_4	1.0	1.0		1.0
HCl	0.13±0.02	0.13±0.02	0.13	0.21
HBr	0.65±0.08	0.68±0.07	0.53	
HI	0.62±0.08	0.74±0.08	0.42	
H_2	0.40±0.05	0.37±0.05		

[a]Based upon comparison of relative $HF^{\dagger}_{vJ}$ emission intensities from CH_4/H_2, CH_4/HCl, CH_4/HBr, and HBr/HI pairs. The last pair gave 1.04 in favor of HBr. These results include the presence of high J levels of $HF^{\dagger}_v$.

[b]Based upon comparison of relative $HF^{\dagger}$ emission intensities but without inclusion of population in high HF J levels.

[c]These rate constant measurements were for each reaction individually. We have tabulated the ratio of 300 K rate constants given in Ref. 16(a) for the HX series; the new measurements from this laboratory[16b] for HBr and HI are higher and in better agreement with our relative rate constants.

the curves change rather abruptly at $J=7$–8 for $v=1$ and 2, and at $J=5$–6 for $v=3$ and 4. For levels above these values, the plots are relatively flat until the rotational energy approaches the mean available energy. It seems plausible that the *initial* $J \leq 6$–8 populations can be estimated by extrapolation of the straight line from the mid-J population, as shown in Fig. 5.

The relaxed components of the low J level populations were obtained by subtracting the extrapolated initial populations from the observed populations. The relaxed component for each v level and its apparent Boltzmann temperature are listed in Table IV. The apparent tem-

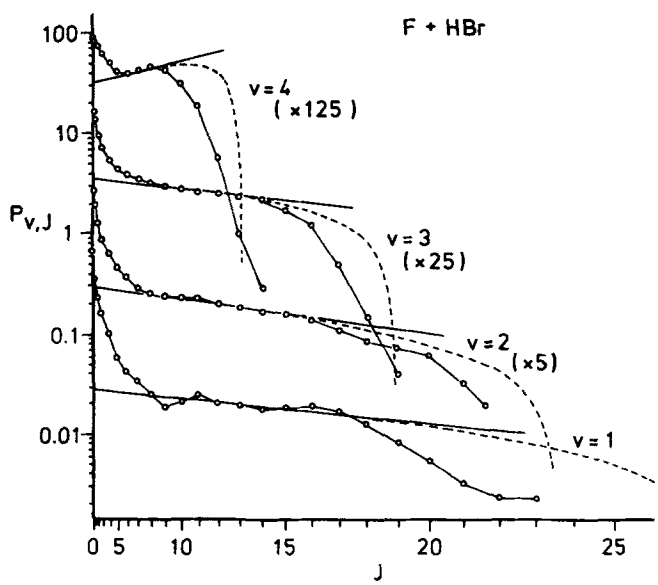

FIG. 5. Plot of $\ln[P_{vJ}/(2J+1)]$ vs $(J)(J+1)$ for each vibrational level of the distribution of experiment 7. The open circles connected by lines represent the observed results. The solid straight lines were fitted to the data points in the mid-J region. The dashed curves are linear surprisal rotational distributions (experiment 8) deduced from the straight lines and maximum available rotational energies. The $v=2$–4 P_{vJ} values were scaled (as shown) to avoid overlapping of curves.

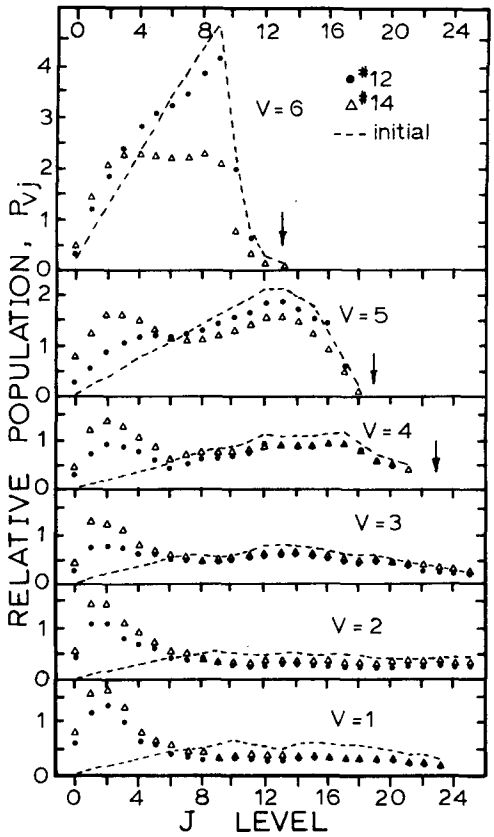

FIG. 6. The HF_{vJ} distributions from F+HI for experiments 12 and 14 of Table I in the cold-wall reactor. The dashed lines are our estimated initial distributions. The $\sum_v \sum_J P_{vJ}$ is normalized to 100 for each experiment. The small vertical arrow indicates the highest energetically allowed J level.

peratures were obtained by fitting a straight line to $J = 0-3$ points of the separated relaxed components on a $\ln[P_{vJ}/(2J+1)]$ vs $J(J+1)$ plot. The deviations of the low J components from a Boltzmann distribution, which is of no physical significance, may be a consequence of the assumptions made in assigning the initial low J populations or possibly be associated with the degree of rotational relaxation. The relaxed component was added equally to the high J levels to obtain initial rotational populations. The final result is shown by the dashed curves in Fig. 4.

D. Vibrational-rotational distributions from HI

Figure 6 shows the distributions from two experiments (#12, 7 μmol/s flow of HI and #14, 100 μmol/s flow of HI). Under these conditions the relative vibrational populations for $v=1-4$ are almost constant although there are some differences, probably due to collisional relaxation with HI, in the rotational distributions. For experiment 14 rotational relaxation is apparent for $v=5$ and even more in $v=6$. The rotational relaxation appears to be mainly depletion of the mid-J levels without much growth in the low J levels, e.g., vibrational relaxation. The $HF^{\dagger}$ vibrational distribution was nearly constant for HI flow rates of 10–30 ml/min; however, experiment 14 suggests that relaxation of $v=6$ may be extremely fast and comparable to rotational relaxation. Such fast vibrational relaxation may explain the low $v=6$ population observed in the flow reactor (Table II). Radiative decay constants[18] for $v=6$ are $A_{6-5}=436$ and $A_{6-4}=271$ s^{-1}. For a 0.2 ms observation time the radiative decay would correspond to a fractional $v=6$ loss of 0.87. In the cold-wall vessel collisional relaxation may be serious at higher flow rates and radiative loss may be more serious for the low flow rates, especially in our large vessel. A narrow range of conditions may be necessary for our cold-wall vessel to obtain the best $v=6$ population. Despite these arguments, we are reluctant to give undue weight to any one experiment and the mean distribution from experiments 12–14 is used as the best vibrational distribution for F + HI.

The lowest flow rate experiment (#11) has increased populations in $v=1$ and 2 and reduced populations in $v=5$ and 6. The increased population in $v=1$ and 2 occurs nearly entirely in rotational levels below $J=7$. The rotational distributions in $v=6$ and 5 closely resemble those shown in Fig. 6 for experiment 12. The $v=3$ and 4 distributions closely resemble those shown for experiment 14. These results are in accord with the variation of P_v(HF) with HBr flow, which already have been discussed in some detail.

Separation of the Boltzmann-like components from the low J levels of the steady-state distributions of Fig. 6 was done in the same way as discussed for the HBr reaction. The fraction of the low J component and its effective temperature are shown in Table IV for each v level. The initial rotational–vibrational distributions obtained by this procedure are shown in Fig. 6 by the dashed curves. The larger Boltzmann component for the lower v levels is especially noticeable for the F + HI reaction. Jonathan and co-workers[8] observed similar results. This greater degree of relaxation possibly may be associated with the higher translational energy of the molecules in low v levels. The high J components observed in the flow reactor for Reactions (3) are not of much aid in identifying the maximum in the $v=1$ and 2 rotational distributions because the distributions are rather flat. For $v=3-5$ the maximum of the high J

TABLE IV. Parameters for describing rotational distributions.

	v	P_v	f_B[a]	T_B (K)[a]	A[b]	B[b]	θ_R[b,c]
HBr	1	0.12	0.38	258	0.38	0.028	0.89
	2	0.17	0.27	281	0.38	0.055	0.87
	3	0.30	0.17	334	0.39	0.133	0.19
	4	0.41	0.23	467	0.49	0.22	−1.5
HI	1	0.10	0.49	247	1.7	0.069	2.7
	2	0.11	0.41	260	1.4	0.060	1.6
	3	0.13	0.21	300	0.70	0.11	1.3
	4	0.16	0.18	362	0.76	0.12	−0.06
	5	0.22	0.13	512	0.44	0.24	−0.58
	6	0.28	0.15	573	0.64	0.72	−0.71

[a]The fraction of the molecules that are in the low J distribution with Boltzmann temperature T_B after subtraction of the extrapolations shown in Fig. 5.

[b]Weighting parameters used in Eq. (9) to describe the steady-state rotational distributions.

[c]Slope in the linear rotational surprisal plot [Eq. (7)].

TABLE V. Comparison of HF vibrational distributions from arrested relaxation cold-wall experiments.

Reaction	Reference	P_v 0	1	2	3	4	5	6
F+HCl	This work		0.25	0.64	0.11			
	8		0.29	0.57	0.14			
	6		0.27	0.57	0.16			
	This work[a]	0.07	0.23	0.60	0.10			
F+HBr	This work		0.14	0.17	0.30	0.39		
	8		0.16	0.19	0.31	0.34		
	7[b]		0.47	0.29	0.14	0.10		
	This work[a]	0.04	0.135	0.165	0.29	0.37		
F+HI	This work		0.11	0.12	0.14	0.17	0.21	0.25
	8		0.10	0.12	0.14	0.19	0.24	0.20
	This work[a]	0.06	0.10	0.11	0.13	0.16	0.20	0.24

[a]The distribution including the estimate for a $v=0$ contribution, which was made from extrapolation of vibrational surprisal plots to $f_v=0$. Since only two significant figures are used, the renormalization of the HI results slightly distorts the relative populations.

[b]Obtained by extrapolation of the relative populations to zero HBr flow rate. For higher flow rates Polanyi and co-workers[7] found $v_1/v_2/v_3/v_4=0.25/0.28/0.28/0.18$.

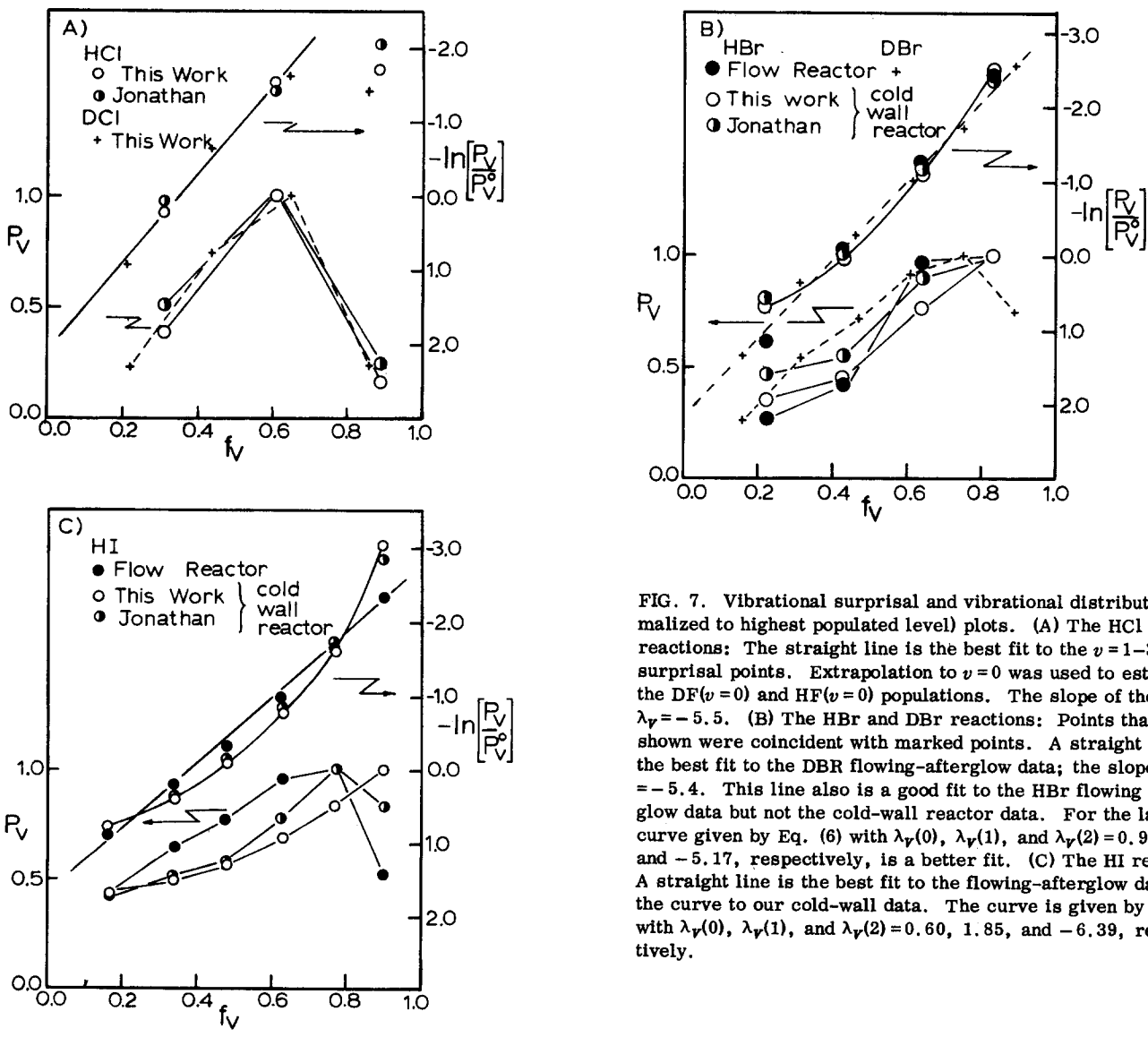

FIG. 7. Vibrational surprisal and vibrational distribution (normalized to highest populated level) plots. (A) The HCl and DCl reactions: The straight line is the best fit to the $v=1$–3 DCl surprisal points. Extrapolation to $v=0$ was used to estimate the DF($v=0$) and HF($v=0$) populations. The slope of the line is $\lambda_v=-5.5$. (B) The HBr and DBr reactions: Points that are not shown were coincident with marked points. A straight line is the best fit to the DBR flowing-afterglow data; the slope is $\lambda_v=-5.4$. This line also is a good fit to the HBr flowing afterglow data but not the cold-wall reactor data. For the latter the curve given by Eq. (6) with $\lambda_v(0)$, $\lambda_v(1)$, and $\lambda_v(2)=0.95$, 1.53, and -5.17, respectively, is a better fit. (C) The HI reaction: A straight line is the best fit to the flowing-afterglow data and the curve to our cold-wall data. The curve is given by Eq. (6) with $\lambda_v(0)$, $\lambda_v(1)$, and $\lambda_v(2)=0.60$, 1.85, and -6.39, respectively.

TABLE VI. Summary of energy disposal.

Molecule	$\langle E\rangle^a$ (kcal/mol)	$\langle f_V\rangle^b$	$\langle f_R\rangle^c$	$\langle f_T\rangle^d$	$\langle g_R^v\rangle^e$ $v=1$	$v=2$	$v=3$	$v=4$	$v=5$	$v=6$	$\langle g_R\rangle^f$	$\langle g_T\rangle^f$
HCl	36.3	0.51	0.18	0.31	0.35	0.41	0.49				0.39	0.61
DCl	37.0	0.52										
HBr	51.0	0.59	0.13	0.28	0.27	0.28	0.35	0.43			0.33	0.67
DBr	51.5	0.58										
HI	67.2	0.59	0.12	0.30	0.20	0.28	0.33	0.38	0.42	0.43	0.32	0.68

[a] $\langle E\rangle = -\Delta H_0^\circ + E_a + (5/2)RT$; $E_a = 2.0$ kcal mol^{-1} for HCl and 1.0 for HBr and HI.
[b] $\langle f_V\rangle = [\sum_v P_v(E_V/\langle E\rangle)]/\sum_v P_v$; these values include $P_{v=0}$ values from Table V.
[c] $\langle f_R\rangle = [\sum_v \sum_J P_{vJ}(E_R/\langle E\rangle)]/\sum_v \sum_J P_{vJ}$; for this calculation P_{0J} was assumed to be the same as P_{1J}.
[d] $\langle f_T\rangle = 1 - \langle f_V\rangle - \langle f_R\rangle$.
[e] $\langle g_R^v\rangle = [\sum_J P_{vJ} E_R/(\langle E\rangle - E_V)]/\sum_J P_{vJ}$.
[f] $\langle g_R\rangle = \langle f_R\rangle/(1-\langle f_V\rangle)$; $\langle g_T\rangle = \langle f_T\rangle/(1-\langle f_V\rangle)$.

components observed in the flow reactor match those of the original distributions shown in Fig. 6.

IV. DISCUSSION

A. Initial vibrational distributions

The results from cold-wall reactor studies of Reactions (1)–(3) are summarized in Table V and in Fig. 7. These values also may be compared to the flow reactor distributions in Table II. All investigators have used Sileo and Cool's rotationless Einstein coefficients[18] to convert the HF line intensities to relative populations, although different vibrational–rotational interaction factors were used in each laboratory. This mainly affects the rotational distributions. All studies agree that the HF† distributions extend to the highest possible rotational levels, at least for the two highest v levels. Before proceeding with the energy disposal analysis, the total available energy from Reactions (1)–(3) is needed. Usually,[1,2] Eq. (5) is used for this purpose:

$$\langle E\rangle = -\Delta H_0^\circ + E_a + 5/2RT \ . \tag{5}$$

The HBr and HI reactions are sixfold faster at room temperature than the HCl reaction, presumably because of a lower activation energy E_a. The factor of 6 corresponds to approximately 1 kcal mol^{-1} difference in E_a and we will use an E_a of 1.0 kcal mol^{-1} for HBr and HI and 2.0 kcal mol^{-1} for HCl. Examination of the highest observed HF_{vJ} levels gives $\langle E\rangle$ of 36.2 ($v=3$, $J=8$), 51.3 ($v=4$, $J=13$) or 51.6 ($v=3$, $J=19$), and 67.9 ($v=6$, $J=12$) or 66.1 ($v=5$, $J=17$) for HCl, HBr, and HI, respectively. These are consistent with the $\langle E\rangle$ of Table VI. Although an E_a of 0.88 kcal mol^{-1} has been reported[20] for F + HCl, recent work[16(b)] shows non-Arrhenius behavior and traditional measurements of E_a may need reinterpretation. The uncertainty in E_a will not seriously affect the definition of $\langle E\rangle$ from Eq. (5).

Our cold-wall reactor data from the HCl reaction, which are reported elsewhere,[1] give a more sharply peaked vibrational distribution than the two other cold-wall experiments. The flowing afterglow experiments also support the more sharply peaked distribution, but all of the data really are in good agreement. The DF distribution from F + DCl virtually matches that for F + HCl, as shown in Fig. 7(a).

Within the experimental uncertainty, our P_v for HBr and HI are in agreement with Jonathan's distributions.[8,19] The P_v(DF) from F + DBr is in general agreement with our initial HF† distribution from HBr. However, the P_v(HF) that Brandt and Polanyi[7] obtained in their cold-wall experiments seriously disagree with our results. The difference is explained by the dependence of P_v(HF) upon HBr flow rate discussed in Sec. IIB. We concluded that the very low flow rate data were not reliable for assignment of initial vibrational distributions. The fast-flow measurements also are an arrested relaxation technique and, providing that the concentrations of reagents are properly controlled, secondary reactions are not important. Under the conditions used for the flowing afterglow experiments, collisions between HF(v) and I or a second HF(v) are negligible at the time of observations (≤ 0.2 ms). We conclude that our and Jonathan and co-workers' distributions are reliable estimates for the initial distributions from the F + HBr and HI reactions at 300 K. Within our data set, the only point of controversy is the $v=6$ population from F + HI. At the present time we favor the result from the cold-wall reactor rather than the lower value from the fast-flow reactor.

Extrapolation of vibrational surprisal plots[21] (see Fig. 7) were used to estimate the relative HF($v=0$) population and the results are shown as the last entry for each reaction in Table V. Although the surprisals may not be strictly linear, the points for the lower v levels are sufficiently linear so that good estimates of the relative $v=0$ populations can be obtained.

The location of the $v=3$ points on the F + HCl surprisal plot is very sensitive to the choice of $\langle E\rangle$. On the basis of Polanyi's data,[6] we previously favored a linear plot.[1,4] However, our more sharply peaked distribution deviates even further from a linear plot. The $v=1$–3 points from F + DCl fall on a straight line [Fig. 7(a)] but the $v=4$ point is well below this line. Unfortunately, the DF($v=4$) point is only slightly less sensitive than the HF($v=3$) point to the choice of $\langle E\rangle$. The new data now suggest that the vibrational surprisal for F + HCl is linear for $f_V \leq 0.7$ with $-\lambda_V = 5.5$ and nonlinear for $f_V \geq 0.9$. It should be noted that the energy limit is more severe for the highest v data point for HCl ($\langle E\rangle - E_3 = 3.8$ kcal mol^{-1}) than for HI ($\langle E\rangle - E_6 = 6.4$ kcal mol^{-1}). If for-

mation of $Cl(^2P_{1/2})$ is important,[5] this seriously interacts with the selection of $\langle E \rangle$ and further clouds the interpretation of the surprisal plot for $f_V \geq 0.9$.

Within the uncertainty of the experimental data [and the complication associated with $Br(^2P_{1/2})$ formation] the HBr vibrational surprisal could be considered linear, especially for the F + DBr and HBr flow reactor data. The slope of the line shown in Fig. 7(b) is $\lambda_V = -5.4$. However, if the cold-wall $v=1$ relative population is considered to be more reliable, a better *empirical* fit to the HBr surprisal plot is given by the polynomial

$$I(f_V) = \lambda_V(0) + \lambda_V(1) f_V + \lambda_V(2) f_V^2 \ . \tag{6}$$

The important point is that the surprisal has *upward* curvature (on our plots) in contrast to the low points for HCl and DCl at high f_V.

The HF vibrational surprisal for the cold wall P_v from F + HI is definitely nonlinear. However, the P_v from the flowing afterglow experiment gives a linear surprisal plot and one should be cautious not to overemphasize the nonlinearity of the HI plot. Nevertheless, based upon our selection of the best distribution there appears to be a systematic variation in the surprisal plots in the HCl, HBr, HI series, as suggested by Jonathan and co-workers. The nonlinear HI plot has been discussed[22] in connection with the formation if $I(^2P_{1/2})$, but, as already pointed out, Reaction (3b) is of negligible importance.[4,8] Angular momentum restrictions, which might suppress the formation of $HF^{\dagger}_{vJ}$ in high J for $v=1$ or 2, can not explain the nonlinear surprisal. Such restrictions would make $\lambda_V(2)$ positive, rather than negative as observed, because the low v populations would be less than the linear surprisal expectation from the higher v levels where angular momentum restrictions would not exist. In fact, the nonlinearity arises because of the increasing tendency for $HF^{\dagger}$ to be formed in the highest levels for the HBr and HI reactions. The slopes of the surprisal plot given by the highest two vibrational points for HBr and HI (cold-wall data) are -8.2 and -11.0, respectively, which are considerably higher than the slopes defined by the lower points. The increase in $\langle f_V \rangle$ of 0.51 to 0.59 also reflects the favoring of higher v levels for HBr and HI. The larger HF vibrational energy disposal may be related to the larger rate constants for HBr and HI. However, there is a considerable difference in the shapes of the HBr and HI distributions and the true explanation probably is not this simple.

B. Rotational distributions

As noted earlier, the $P_{vJ}/(2J+1)$ vs $J(J+1)$ plots are almost flat in the mid-J regions, as would be expected for statistical rotational distributions. The statistical, or prior, rotational distribution for a three-body reaction is expressed by

$$P_S^0(g_R) = (2J+1)(1-g_R)^{1/2} \tag{7}$$

and a linear surprisal distribution is given by

$$P_{LS}(g_R) = P_S^0(g_R) \exp(-\theta_R g_R) \ . \tag{8}$$

The reduced variable g_R is $f_R/(1-f_V)$, where f_V pertains to the vibrational level in question. In order to avoid introduction of possible bias into the fitting, we first made a comparison to the steady-state distributions from HBr. In Fig. 5, $P_{LS}(g_R)/(2J+1)$ is superimposed on the experimental steady-state population; θ_R was selected so that the curve fitted the observed points in the mid-J region for each v. From the figure it is evident that for each v level the *steady-state* low and mid-J populations can be fitted by the sum of a Boltzmann plus a linear surprisal distribution as follows:

$$P_{vJ} = (2J+1)[A \exp(-E_J/kT_B) + B(1-g_R)^{1/2} \exp(-\theta_R g_R)] \ . \tag{9}$$

The effective temperatures and the other parameters are listed in Table IV. The θ_R values from F + HBr are small, indicating that the distributions are close to statistical in nature. The deviation between observed and linear surprisal distributions is significant for the high J levels and the observed distribution drops below the surprisal distribution as $E_R \to \langle E \rangle$.

The synthesized populations by Eq. (9) with the parameters in Table IV (which were deduced from a plot like Fig. 5) are directly compared with the observed HF_{vJ} population from F + HI in Fig. 8. The apparent deviation at $J=5$–8 from the steady state may be due to the poor approximation of the Boltzmann distribution rather than the possibility of the second maximum in the initial distribution. Although some deviations are seen in higher J regions, they are not significant and the initial distributions are well expressed by the linear surprisal distribution for the HI reaction. The plot similar

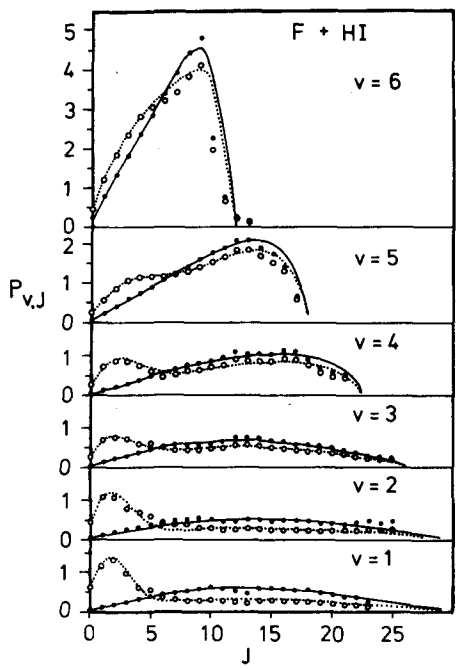

FIG. 8. Comparison of experimental, estimated initial, and simulated HF_{vJ} distributions from F + HI. Open circles are the observed distributions of experiment 12 and the dotted curves are the simulated distributions of Eq. (9) (Boltzmann + linear surprisal). The filled circles are the estimated initial distributions and the solid curves are the simulated fits using only the linear surprisal part of Eq. (9).

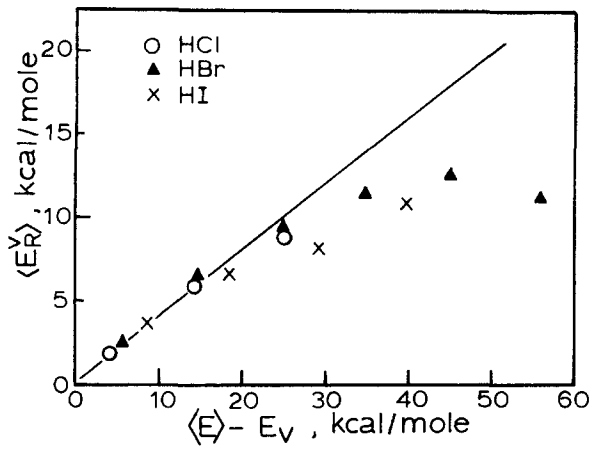

FIG. 9. Plot of $\langle E_R^v \rangle$ vs $\langle E \rangle - E_V$ for the HCl, HBr, and HI reaction. The line shows the expected $\langle E_R^v \rangle$ for statistical partitioning of $\langle E \rangle - E_V$ between E_R and E_T.

to Fig. 8 for F + HBr (not shown) also exhibits a good fit to the linear rotational surprisal, but the agreement for the high J levels is somewhat less perfect than for F + HI. The θ_R values change from positive to negative with increasing v for both HBr and HI.

The rotational distributions from F + HCl[1,6] are concentrated in a more narrow region of J than for Reactions (2) and (3) and the HCl distributions give the poorest fit to a linear rotational surprisal and HCl has the highest HF rotational energy disposal. The reason that rotational distributions from Reactions (1) can be arrested more easily than from Reactions (2) or (3) is because the HF† distribution is localized in a few levels around $J = 10$–15.

Another way to compare the rotational distributions is to examine the most probable rotational energy of each v level. For HCl, g_R^{mp} is about 0.5 and is constant for $v = 1$, 2, 3, as pointed out before.[1,14] However, g_R^{mp} is 0.66 (0.52) in the highest level and ~0.24 (0.38) in the lowest level for HI(HBr). Since P_{vJ} is very broad for the lower v, g_R^{mp} is not the best way to examine these distributions. We prefer to use $\langle g_R^v \rangle$ or $\langle E_R^v \rangle$. The $\langle g_R^v \rangle$ values are shown in Table VI and $\langle E_R^v \rangle$ is plotted vs $\langle E \rangle - E_V$ in Fig. 9. The variation in $\langle g_R^v \rangle$ is largest for the most exoergic reaction. The plot clearly shows that $\langle E_R \rangle$ is ~40% of the energy available to that particular level for $\langle E \rangle - E_V \lesssim 25$ kcal mol^{-1}; however, for higher available energies $\langle E_R^v \rangle$ deops below this fraction. The 40% partitioning of $\langle E \rangle - E_V$ to E_R is the statistical expectation.

C. Summary and discussion of energy disposal

A systematic investigation has been made of the energy disposal for the F + HCl, HBr, and HI reactions at room temperature. By combining the best features of the cold-wall, arrested vibration–rotation relaxation technique and the fast-flow, arrested vibration relaxation technique, a set of initial vibrational–rotational populations is recommended. Less extensive data for the F + DCl and DBr reactions were presented to support the results of the other reactions. Although Cl($^2P_{1/2}$) and Br($^2P_{1/2}$) probably are formed in about 10% of the reaction events,[4(a),5,7] there is little evidence that formation of the upper spin–orbit halogen state plays a major role in the energy disposal. The present work provides no further insight into the mechanism for X($^2P_{1/2}$) formation and this aspect will not be discussed further.

Using the initial distributions, triangle plots were made (see Fig. 10). The most obvious change in the series is the shift of the highest peak into the upper left hand corner as the halogen becomes heavier. This also is reflected in the small increase in $\langle f_V \rangle$. The small increase in $\langle f_V \rangle$ seems to come at the expense of $\langle f_R \rangle$ resulting in a nearly constant $\langle f_T \rangle$. Such apparent conservation of translational energy, however, does not hold for individual vibrational states and the fraction of translational energy increases with decreasing v for all three reactions (see Table VI). This trend also is illustrated by the shapes of the contour plots for HF($v = 1$) from HBr and for HF($v = 1$ and 2) from HI. On the basis of previously published data, the vibrational surprisals for F + HCl and F + HBr appeared to be linear.[1,4] However, the detailed evaluation of the newer data suggests some deviation from linearity, especially for HCl and HI. Thus, the pleasing simplicity[23] of the vibrational energy disposal for the X + HX′ series, although still present at the qualitative level, tends to disappear upon detailed inspection. This newly found complexity may spoil the use of the F + HX series as reference reactions against which to compare the energy disposal for F + polyatomic RH reactions,[2,23] although for this purpose the qualitative features probably still are the more important. The complexity for the vibrational energy disposal carries over to the rotational energy disposal. The least exoergic reaction F + HCl closely follows the statistical expectation with ~0.40 ($\langle E \rangle - E_V$) being released as $\langle E_R^v \rangle$; however, the distributions are more sharply peaked than the statistical distributions. The two more exoergic reactions show a trend of decreasing fraction of rotational energy being released to the lower v levels. This trend could be an effect of angular momentum restrictions associated with formation of the higher ($J \geq 15$) rotational levels. However, the existence of two channels for HF† formation, which also may involve different angular momentum restrictions, is a more likely explanation.

The non-Arrhenius temperature dependence[16(b),24] of the X + HX′ reactions has been interpreted as evidence for two product formation channels. One channel corresponds to direct reaction upon approach of X to the H end of the molecule. The second channel may correspond to approach of X to the X′ end with subsequent formation of a bound complex (HX′X) and eventual rearrangement to HX + X′. The second channel, with an effective negative temperature coefficient, probably is more important when X′ is I or Br since those complexes are expected to be more strongly bound.[25] The molecular beam study[26] of Cl and Br with HAt is especially important in this context because the angular HCl and HBr distributions were nearly symmetric about 90°, and long-lived "complexes" certainly are implied for these reactions. There already is strong evidence in the lit-

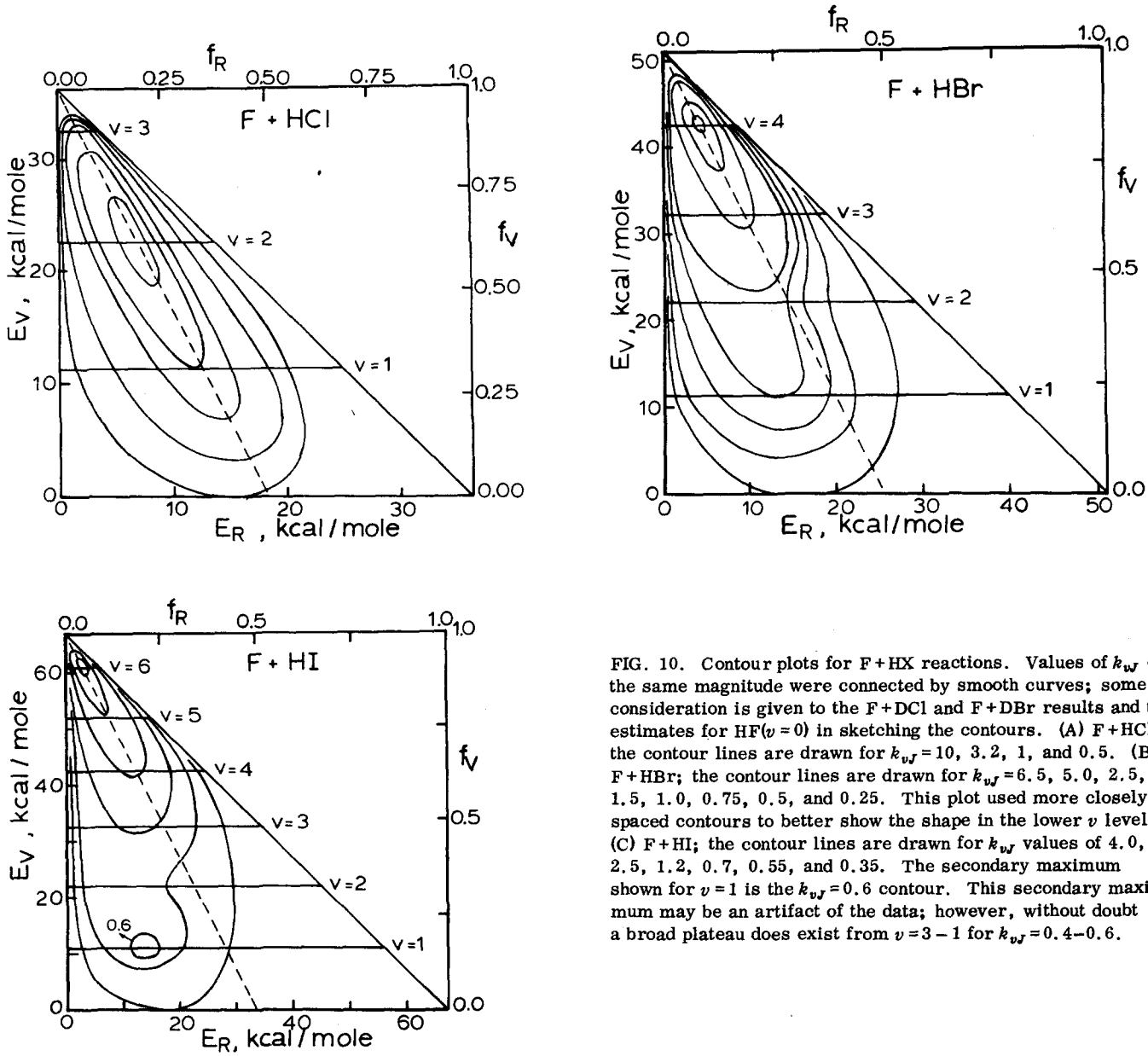

FIG. 10. Contour plots for F+HX reactions. Values of k_{vJ} of the same magnitude were connected by smooth curves; some consideration is given to the F+DCl and F+DBr results and to estimates for HF($v=0$) in sketching the contours. (A) F+HCl: the contour lines are drawn for $k_{vJ}=10$, 3.2, 1, and 0.5. (B) F+HBr; the contour lines are drawn for $k_{vJ}=6.5$, 5.0, 2.5, 1.5, 1.0, 0.75, 0.5, and 0.25. This plot used more closely spaced contours to better show the shape in the lower v levels. (C) F+HI; the contour lines are drawn for k_{vJ} values of 4.0, 2.5, 1.2, 0.7, 0.55, and 0.35. The secondary maximum shown for $v=1$ is the $k_{vJ}=0.6$ contour. This secondary maximum may be an artifact of the data; however, without doubt a broad plateau does exist from $v=3-1$ for $k_{vJ}=0.4$–0.6.

erature for a migratory pathway involving HX'X, as well as direct pathway, for reaction of H with X'X to yield HX.[27–29] The direct pathway gives relatively low HX vibrational and rotational excitation, whereas the migratory channel gives higher HX excitation. On contour plots such as those shown in Fig. 10, the migratory channel often can be identified as a second ridge at much higher E'_R than the direct pathway. This general pattern has been verified for H+BrF in the most recent study of the XX' series from Polanyi's laboratory.[29] The migratory channel is less important for both ClF and IF than for BrF. In contrast to the H+FX series, the rotational energy disposal for the F+HX series does not show evidence for a second channel at high E'_R. This is especially puzzling for F+HBr because the migratory (complex) channel is so important for H+FBr. However, for the latter the available energy is 78 kcal mol^{-1}, whereas for F+HBr the energy is only 48 kcal mol^{-1}. This energy difference and the method of HBrF formation *may* affect the energy disposal of the migratory pathway from H+BrF vs F+HBr.

The possibilities for F+HI and H+FI can be best summarized by the diagram (and thermochemistry) below:

$$\begin{array}{ccc} \mathrm{F+HI} & \xrightarrow{\text{direct}} & \mathrm{FH^{\dagger}+I}\,, \quad \Delta H^{\circ}_0 = -64.7\ \text{kcal mol}^{-1}\,, \\ & \searrow \nearrow \uparrow \text{direct} & \\ & \mathrm{HIF^{*} \rightleftharpoons IF+H}\,, & \Delta H^{\circ}_0 = 5\ \text{kcal/mol}^{-1}\,. \end{array}$$

The HIF* complex lies 26 kcal mol^{-1} below F+HI, but still 38 kcal mol^{-1} above the HF+I exit channel.[25] The migratory pathway was less important than the direct pathway for HF formation from H+IF. The diminished importance of migration for H+IF was attributed[29] to the low available energy for the HI+F exit channel, which tends to inhibit the "insertion" of the H between the I and F atoms. This insertion is the prelude to migration.[27] The fact that HIF* actually is an observed[25]

species also shows that a significant barrier exists for HF formation from the HIF geometry. Brandt and Polanyi estimated the HI/HF product ratio to be ≥ 28 so there is little doubt about the importance of the HIF pathway for H + IF. According to detailed balance, HIF* will be formed by F + HI; the question is whether or not migration of H to give HF + I occurs.

Identification of a second component from the rotational populations from F + HX may be thwarted by the broad $HF^{\dagger}$ rotational distribution from the direct reaction. The observed $HF_{v,J}$ distributions for HI and HBr *could* be the result of superposition of two components that fortuitously resemble a statistical partitioning between rotational and translational energies for a fixed v. The much sharper rotational distributions from HCl are of interest in this context. Jonathan found that trajectory calculations on a repulsive surface *overestimated* the rotational energy disposal, so the presence of a second channel of lower rotational energy could explain the difference in the calculated vs observed $HF^{\dagger}$ rotational distributions. The other major problem with the calculations was a poor match with the magnitude of the rate constant.

The answer to the following question is crucial for the suggestions in the above paragraphs. Can the migratory channel give a lower rotational component for F + HX, such as is suggested for $v=1$ and 2 in Fig. 10(c), but a higher rotational component for H + FX? The answer is a qualified perhaps. For H + FX, the HF migratory channel initially involves formation of the XH bond with subsequent transfer of the H as the X and F are trying to separate.[27] For the F + HX case the HXF* complex will be formed with some release of potential energy (presumably 26 kcal mol^{-1} for HIF), but the XH bond is not expected to acquire much specific localized excitation and, in particular, there is no obvious mechanism for release of rotational energy in complex formation. Thus, the dynamics associated with H migration for the two cases are different. The energy disposal by the migratory channel for FXH formed by association of F and XH may be more akin to statistical energy release and favor lower f_V and f_R than the direct reaction; there is a suggestion of such behavior in Figs. 10(b) and 10(c).

If the $HF^{\dagger}$ product is formed by both direct and complex channels and if both halogen spin–orbit states are reaction products for Reactions (1) and (2), as currently thought, then interpretation of the energy disposal data for these three-body reaction becomes fraught with difficulty. Rather than dwelling on the relatively small differences in the energy disposal for HCl, HBr, and HI, the main question becomes why is the HF energy disposal so similar for the F + HX series and for many other F + HR (R = polyatomic) reactions,[23] if two different channels are operative for HX? Possibly the $HF^{\dagger}$ at 300 K mainly arises from the direct reaction and the small difference in energy disposal for the series reflect minor (and different) contributions from the HXF channel. Before more definitive conclusions can be drawn, the energy disposal for the direct and complex channels must be separated and identified. On the basis of the interpretation of the variation of the rate constants with temperature,[16(b)] this should be possible by infrared chemiluminescence studies at variable temperature. One point to remember is that the trajectories for the F–H–X mass combination exhibit "complex-like" behavior even on a purely repulsive surface.[8] The presence of a potential well associated with the FXH configuration may serve to enhance that aspect of the dynamics without causing a radical change in the energy disposal.

The observed dependence of the $HF(v,J)$ populations on the HBr and HI flow rates probably is not correlated with a variation of the amount of reaction proceeding by the direct and complex pathways. It is unlikely (although not impossible) that changing the reagent flow rate results in selection of reactant states (or variation of temperature) in some way such that one of the two channels was favored. The most positive evidence against such an argument is that a similar variation of $HF(v,J)$ populations with polyatomic reagent flow rate was observed for cases in which the possibilities of two channels for HF formation are not so obvious (see Table I). At this time we favor the explanation offered in the text to explain the abnormal variation of the $HF(v,J)$ populations with low reagent flow rates in the cold-wall reactor.

Note added in proof: In response to the suggestions made in this paper concerning the possible role of "background" flow rates on the $HF(v)$ populations from the cold-wall arrested relaxation experiments, L. W. Dickson and J. C. Polanyi (private communication) have repeated the low HBr flow experiment (Expt. 8) reported in Ref. 7. Their finding that $k(v')$ increases steadily toward lower v' is unaffected by addition of ~ 10× excess of Ar or of (undissociated) SF_6.

ACKNOWLEDGMENTS

This work was supported by the National Science Foundation (Grant 77-21380). We thank Dr. Wickramaratchi for permission to include his experiments with F + DCl and F + DBr in this paper. We also thank Professor Houston and Professor Polanyi for sending preprints of Refs. 16(b) and 7, respectively, and Dr. Grover for a discussion of the HAt reactions and for his views on the complex channel of X + HX′ reactions.

[1] D. J. Bogan and D. W. Setser, in "Fluorine Containing Free Radicals Reaction Kinetics and Dynamics," Am. Chem. Soc. Symp. Ser. **66**, 237 (1978).
[2] D. J. Bogan and D. W. Setser, J. Chem. Phys. **64**, 586 (1976).
[3] D. J. Bogan, D. W. Setser, and J. P. Sung, J. Phys. Chem. **80**, 888 (1977).
[4] (a) J. P. Sung and D. W. Setser, Chem. Phys. Lett. **48**, 413 (1977). In this work the rate constants are based upon measurements made with the monochromator, but the best populations were deduced from our first experiments with the interferometer. Subsequently, our technique has improved for both types of measurements. (b) J. P. Sung and D. W. Setser, J. Chem. Phys. **69**, 3868 (1978).
[5] W. Nip and M. A. A. Clyne, Int. J. Chem. Kinet. **10**, 365 (1977).
[6] A. M. C. Ding, L. J. Kirsch, D. S. Perry, J. C. Polanyi, and J. L. Schreiber, Faraday Discuss. Chem. Soc. **55**, 252

(1973).
[7]D. Brandt, L. W. Dickson, L. N. Y. Kwan, and J. C. Polanyi, Chem. Phys. **39**, 189 (1979).
[8]P. Beadle, M. R. Dunn, N. B. H. Jonathan, J. P. Liddy, and J. C. Naylor, J. Chem. Soc. Faraday Trans. 2 **74**, 2170 (1978).
[9]J. P. Sung, R. J. Malins, and D. W. Setser, J. Phys. Chem. **83**, 1007 (1979).
[10]R. J. Malins and D. W. Setser, J. Chem. Phys. (in press).
[11]J. P. Sung and D. W. Setser, Chem. Phys. Lett. **58**, 98 (1978).
[12]K. Tamagake and D. W. Setser, J. Phys. Chem. **83**, 1000 (1979).
[13](a) K. Tamagake, D. W. Setser, and W. G. Fateley, "International Conference on Fourier Transform Spectroscopy (1977), reprints are available. (b) K. Tamagake, Appl. Spectrosc. Lett. (to be submitted).
[14]D. J. Smith, D. W. Setser, K. C. Kim, and D. J. Bogan, J. Phys. Chem. **80**, 898 (1977).
[15]I. Burak and M. Eyal, Chem. Phys. Lett. **52**, 534 (1977).
[16](a) E. Wurzberg, A. J. Grimley, and P. L. Houston, Chem. Phys. Lett. **57**, 373 (1978). (b) E. Wurzberg and P. L. Houston, J. Chem. Phys. **72**, 5915 (1980).
[17]B. Dill and H. Heydtmann, Chem. Phys. **35**, 161 (1978).
[18]R. N. Sileo and T. A. Cool, J. Chem. Phys. **65**, 117 (1976).
[19]N. B. H. Jonathan (private communication). The flow rates used for the experiments of Ref. 8 correspond to the midrange of flow rates used in our work.
[20]S. H. Mo, E. R. Grant, F. E. Little, R. G. Manning, C. A. Mathis, G. S. Werre, and J. W. Root, "Fluorine Containing Free Radicals Kinetics and Dynamics of Reactions," Am. Chem. Soc. Symp. Ser. **66**, 59 (1978).
[21]R. B. Bernstein and R. D. Levine, Adv. At. Mol. Phys. **11**, 216 (1975).
[22]U. Dinur, R. Kosloff, R. D. Levine, and M. J. Berry, Chem. Phys. Lett. **34**, 199 (1975).
[23]B. E. Holmes and D. W. Setser, in *Physical Chemistry of Fast Reactions*, edited by I. W. Smith (Plenum, New York, 1980), Vol. 2.
[24]C.-C. Mei and C. B. Moore, J. Chem. Phys. **67**, 3936 (1977); **70**, 1759 (1979).
[25]J. J. Valentini, M. J. Coggiola, and Y. T. Lee, J. Am. Chem. Soc. **98**, 853 (1976); Faraday Discuss. Chem. Soc. **62**, 232 (1977).
[26]J. R. Grover, C. R. Iden, and H. V. Lilenfeld, J. Chem. Phys. **64**, 4657 (1976).
[27]J. C. Polanyi, J. L. Schreiber, and W. J. Skrlac, Faraday Discuss. Chem. Soc. **67**, 66 (1979) and references listed here.
[28]J. P. Sung, R. J. Malins, and D. W. Setser, J. Phys. Chem. **83**, 1007 (1979).
[29]D. Brandt and J. C. Polanyi, Chem. Phys. **45**, 65 (1980).